# NUMERICAL MODEL FOR SURGE & SWAB PRESSURES ON WELLS WITH CROSS-SECTION VARIATION

**João Victor Fedevjcyk, joaovictor88@gmail.com**
**Silvio Luiz de Mello Junqueira, silvio@utfpr.edu.br**
**Cezar Otaviano Ribeiro Negrão, negrao@utfpr.edu.br**
UTFPR - Federal University of Technology - Parana – Av. Sete de Setembro, 3165, CEP 80.230-901 – Curitiba-PR-Brazil

*Abstract. Drilling is one of the most complex steps in petroleum exploration. The process is accomplished by rotating a drill bit to compress the rock formation. During drilling, a fluid is pumped into the well to lubricate and cool down the drill bit, to clean up the well, to avoid the formation fluid influx to the well and also to stabilize the borehole walls. Fluid circulation, however, can be interrupted for maintenance reasons and the drill pipe can be moved to remove the drill bit. The downward or upward movement of the drill pipe displaces the fluid within the well causing either under pressure (swab) or over pressure (surge), respectively. If the pressure at the well bore overcomes the formation fracture pressure, a loss of circulation can take place. On the other way round, the upward movement may reduce the pressure below the pore pressure and an inflow of fluid to the well (kick) can occur. An uncontrolled kick may cause a blowout with serious damages. The transient flow induced by the axial movement of the drill pipe is responsible for the pressure changes at the well bore. Nevertheless, the well bore cross section variation may modify the pressure change within the pipe. In this paper, the effects of diameter variation of the drilling well on the surge and swab pressures are investigated. The equations that represent the phenomenon (mass and momentum conservation) are discretized by the finite volume method. Despite its non-Newtonian properties, the fluid is considered Newtonian in this first work. The drill pipe is considered closed and the flow is assumed as single-phased, one-dimensional, isothermal, laminar, compressible and transient. A sensitivity analysis of the flow parameters is carried out. The cross-section changes cause the reflection of the pressure wave, and consequently pressure oscillations.*

*Keywords: Surge & swab pressures, drilling fluid, annular flow, compressible flow, transient flow*

## 1. INTRODUCTION

Each stage of the drilling process uses a smaller bit diameter than the previous one because of the continuous cementing of the well bore. Additionally, the drill pipe does not have the same diameter along its axis because of the accessories. Figure 1 shows the configuration of the well.

When the drill pipe is moved downward the drilling fluid is compressed and the borehole pressure increases. If this surge pressure overcomes the formation fracture pressure a rupture of the wellbore walls may happen and the drilling fluid may be lost. On the other hand, the upward movement of the drill pipe decreases the inside well pressure. This is known as swab and if the pressure falls down below the pore pressure, formation fluid can flow into the well (kick). An uncontrolled kick can even cause a blowout.

Several studies were conducted to predict the surge and swab pressures. These studies were based on the conservation equations of mass and momentum and can be divided into steady-state and dynamic models. Steady-state models, such as Burkhardt (1961), Fontenot and Clark (1974), Bourgoyne et al. (1991), Bing et al (1995) and Sampaio Jr. (2002), considered only the effects of viscous flow. However, in dynamic models, such as Lal (1983), Mitchell (1988), Bing and Kaiji (1996), Kimura (2008) and Almeida (2009), both viscous and inertial effects are taken into account.

The current paper investigates the effects of the variation of the cross sectional area of oil wells in the surge and swab pressures. The governing equations are discretized by the Finite Volume Method (FVM) (Patankar, 1980) and they were solved iteratively.

## 2. MATHEMATICAL MODEL

Figure 2 shows that an annular space is formed when the drill pipe is introduced into the well. $D_p$ and $D_h$ are the drill pipe and hole diameter, respectively. The well length is $L$, the origin of the coordinate system is place at the well bottom. In this case the drill pipe is considered to move downwards a constant velocity ($V_p$).

The transient flow is assumed to be laminar, isothermal and one-dimensional, and the compressibility is considered to be constant. The borehole is vertical and the fluid is Newtonian. The bottom of the drill pipe is closed and therefore the drilling fluid flows only through the annular space. The well bore is assumed impermeable. The mathematical model is represented by the conservation equations of mass and momentum.
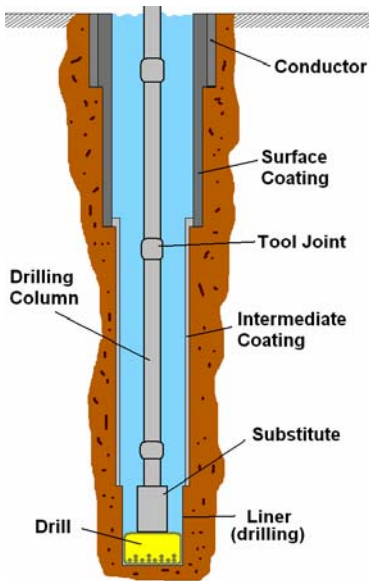
Figure 1. Schematic configuration of the oil well while drilling.
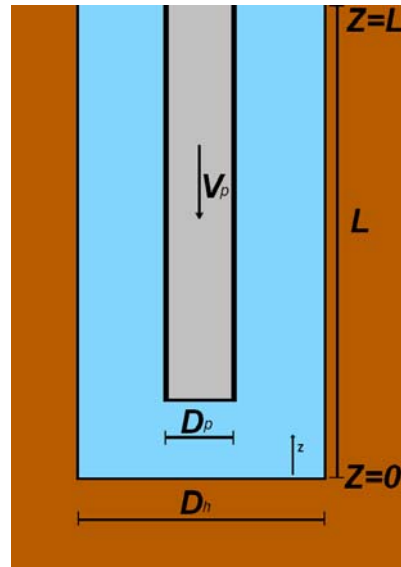


Figure 2. Annular space geometry.

## 2.1 Governing Equations

The mass conservation equation can be written as:

$$\frac{\partial(\rho \overline{V})}{\partial z} + \frac{\partial \rho}{\partial t} = 0 \tag{1}$$

and the momentum conservation equation as:

$$\frac{\partial(\rho \overline{V})}{\partial t} + \frac{\partial(\rho \overline{V}\overline{V})}{\partial z} = -\frac{\partial P}{\partial z} + \frac{\pi}{A_t}(D_h \tau_h - D_p \tau_p) - \rho g \tag{2}$$

where $\rho$ is the fluid density, $\overline{V}$ is the fluid average velocity, $P$ is the pressure, $A_t$ is the cross-section area of annular space, $g$ is the gravity acceleration, and $\tau_h$ and $\tau_p$ are the shear stress at the external and internal walls, respectively. $t$ is the time and $z$ is the axial position.

The shear stress is approximated for the fully developed Newtonian flow:

$$D_p \tau_p + D_h\left(-\tau_h\right) = \frac{8\mu \ln(\beta)(1-\beta^2)}{\ln(\beta)\left(1+\beta^2\right)-\beta^2+1}\overline{V} - \frac{4\mu\left[1-\beta^2+2\beta^2\ln(\beta)\right]}{\ln(\beta)\left(1+\beta^2\right)-\beta^2+1}V_p \tag{3}$$

where $\beta$ is the diameter ratio ($\beta = D_h / D_p$).

Pressure is related to density by the following state equation (Anderson, 1990):

$$P = P_{atm} + \frac{1}{\alpha}\ln\left(\frac{\rho}{\rho_{atm}}\right) \tag{4}$$

where $\alpha$ is the fluid compressibility and the subscript *atm* indicates the atmospheric condition.

To decrease the number of variables, the governing equations are normalized by employing the dimensionless parameters shown in Table 1.

The dimensionless form of the state equation and the conservation equations of mass and momentum are thus written, respectively, as:

$$P* = P*_{atm} + \frac{1}{\alpha *} \ln \rho * \tag{5}$$

$$\frac{\partial(\rho * V*)}{\partial z *} + \frac{\partial \rho *}{\partial t *} = 0 \tag{6}$$

$$\frac{\partial(\rho * V*)}{\partial t *} + \frac{\partial(\rho * V * V*)}{\partial z *} = -\frac{\partial \rho *}{\partial z *} - \frac{1}{Fr} \rho * -$$
$$-\frac{RA}{Re}\left( \frac{16\left[1 - \beta^2 + 2\beta^2 \ln(\beta)\right](\beta - 1)}{\left(\ln(\beta)(1+\beta^2) - \beta^2 + 1\right)(1+\beta)} - \frac{32\ln(\beta)(1-\beta^2)(1-\beta)(\beta - 1)}{\ln(\beta)(1+\beta^2) - \beta^2 + 1}\overline{V}* \right) \tag{7}$$

The dimensionless groups in equations (5), (6) and (7) are defined in Table 2.

Table 1. Dimensionless parameters.

| Dimensionless parameters | Definition |
|---|---|
| Position | $z* = \dfrac{z}{L}$ |
| Time | $t* = t\dfrac{V_p}{L}$ |
| Average Velocity | $\overline{V}* = \dfrac{\overline{V}}{V_p}$ |
| Density | $\rho * = \dfrac{\rho}{\rho_{atm}}$ |
| Pressure | $P* = \dfrac{P}{\rho_{atm}V_p^2}$ |

Table 2. Dimensionless groups.

| Dimensionless groups | Definition |
|---|---|
| Aspect Ratio | $RA = \dfrac{L}{(D_h - D_p)}$ |
| Reynolds Number | $Re = \dfrac{\rho_{atm}V_p(D_h - D_p)}{\mu}$ |
| Froude Number | $Fr = \dfrac{V_p^2}{gL}$ |
| Dimensionless Compressibility | $\alpha * = \alpha\rho_{atm}V_p^2$ |

Equations (8) to (10) are the initial conditions of velocity, density and pressure, respectively:

$$\overline{V}*(z*,t* = 0) = 0 \tag{8}$$

$$\rho *(z,t* = 0) = \frac{1}{1 - \dfrac{\alpha *}{Fr}(1 - z*)} \tag{9}$$

$$P*(z,t* = 0) = P_{atm}* + \frac{1}{\alpha *}\ln\left[\frac{1}{1 - \dfrac{\alpha *}{Fr}(1 - z*)}\right] \tag{10}$$

The flow displaced by the drill pipe is taken as boundary condition at the bottom hole. The fluid average velocity at the bottom hole is thus defined as:

$$\overline{V}*(z = 0,t) = \frac{\beta^2}{1 - \beta^2} \tag{11}$$

The density is constant and equal to its atmospheric condition value in the upper boundary. It value is computed as:

$$\left.\frac{\partial(\rho * \overline{V}*)}{\partial z *}\right|_{z*=1} = 0 \tag{12}$$

## 3. NUMERICAL MODEL

The governing equations are discretized by the Finite Volume Method (Maliska, 2004) and the discretization scheme is illustrated in Figure 3.



Figure 3. Discretization scheme.

The density and pressure variables are placed at the finite volume boundaries and the velocity is located at the center of the control volumes. The grid is uniform with a constant $\Delta z$. The change of cross sectional area is always placed in the middle of a velocity volume, which means that this finite volume has two different diameters.

The discretized momentum conservation equation can be written as:

$$\left[\left(\rho * \bar{V} *\right)_{I'}^{n+1} - \left(\rho * \bar{V} *\right)_{I'}^{n}\right]\Delta z * + \left[\left(\rho * \bar{V} * \bar{V} *\right)_{i'+1}^{n+1} - \left(\rho * \bar{V} * \bar{V} *\right)_{i'}^{n+1}\right]\Delta t * = -\left(P *_{i'+1}^{n+1} - P *_{i'}^{n+1}\right)\Delta t * -$$

$$-\frac{1}{Fr}\rho *_{I'}^{n+1} \Delta z * \Delta t * -\left(\frac{RA_1}{Re_1} + \frac{RA_2}{Re_2}\right)\cdot\left(\frac{16\left[1-\beta^2 + 2\beta^2 \ln(\beta)\right](\beta-1)}{\left(\ln(\beta)\left(1+\beta^2\right)-\beta^2 +1\right)(1+\beta)} - \frac{32\ln(\beta)(1-\beta^2)(1-\beta)(\beta-1)}{\ln(\beta)\left(1+\beta^2\right)-\beta^2 +1}\bar{V} *_{I'}^{n+1}\right)\Delta z * \Delta t * \tag{13}$$

where

$$RA_i = \frac{L_i}{D_{h_i} - D_p} \tag{14}$$

$$Re_i = \frac{\rho_{atm}V_p(D_{h_i} - D_p)}{\mu} \tag{15}$$

$$\beta_i = \frac{D_{h_i}}{D_p} \tag{16}$$

Subscript 1 and 2 refer to downwind and upwind cross sectional areas, respectively. The local pressure drop through the change of the cross-section is written as:

$$\left(P*_{i'+1} - P*_{i'}\right) = -\left(1 - J\frac{A_1}{A_2}\right)^2 \rho*_{I'} \overline{V}*_{I'}^2 - \left(P*_{i'+1} - P*_{i'}\right) \tag{17}$$

where $J$ is a coefficient of local pressure drop. If the variation on cross-section is an expansion then $J = 1$, on the other hand, if it is a contraction, $J = -1.52\left(\frac{A_1}{A_2}\right)^3 + 2.19\left(\frac{A_1}{A_2}\right)^2 - 1.22\left(\frac{A_1}{A_2}\right) - 0.135 + 1.685\left(\frac{A_1}{A_2}\right)^{-1}$ (Assy, 2004).

## 4. RESULTS

First of all, a grid size analysis is carried out. Secondly, the effect of a cross section change is studied and finally, a sensitivity analysis of the dimensionless groups is conducted.

### 4.1 Grid Test

A sensitivity analysis of the grid size is first conducted for a reference case. In all simulations, a well bore with one change on cross sectional area is studied. The variation is placed in the middle of the well. The reference values of dimensionless variables are $\alpha* = 1.27 \times 10^{-6}$, $RA_1 = 10000$, $RA_2 = 6666$, $Re_1 = 400$, $Re_2 = 600$, $\beta_1 = 0.25$ and $\beta_2 = 0.1818$. According to Fortuna (2000), time and space grids have to satisfy the Courant-Fredrichs-Lewy (CFL) criterion because of the hyperbolic characteristic of the governing equations. The CFL number is kept equal to 0.5 for all case studies.

Three numbers of grid cells were tested: 10, 200 and 800 volumes and the results are shown in Figures 4 and 5. The pressure and velocity fields become insensitive to the grid size for 200 finite volumes as the 200 and 800 finite volume results are quite close. Therefore, a 200-volume-grid is used for the simulations hereafter.
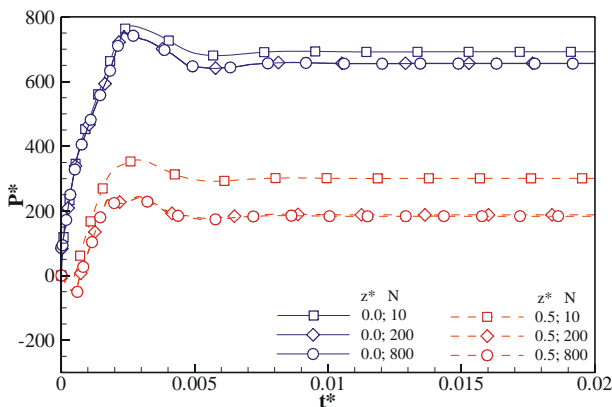


Figure 4. Time change of pressure for three grid sizes at the borehole bottom and immediately after the variation of the cross sectional area.
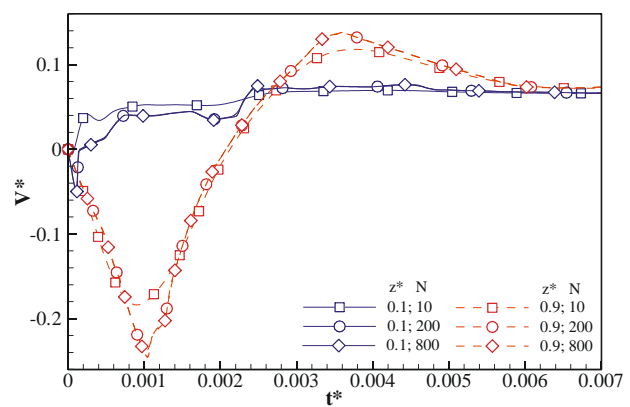


Figure 5. Time change of velocity for three grid sizes close to the borehole bottom and close to the upper end.

### 4.2 Geometric Analysis

The analysis of the effect of the cross-section change is now conducted. The results of a two-cross-section well are compared to those of a one-cross-section well. The later was obtained by Kimura (2008). In the cross-section change case, two situations were considered: an expansion and a contraction. Table 3 shows the dimensionless parameters of these three boreholes and the results are shown in Figures 6 and 7.

Due to pressure wave reflections at the cross-section change, the well with expansion presents pressure peaks over the steady state. Besides, pressure drops at the cross-section change causes valleys of pressures. On the other hand, in wells with contraction, valleys and peaks of pressure are not seen.

Figure 8 shows the average velocity field for the three geometries at two different instants. Note that the average velocity decreases at the contraction and increases at the expansion because of the pressure increase and decrease, respectively. Figure 9 shows there is a peak on the value of the average velocity for wells with an expansion because of

pressure wave reflection at the upper part of the well. This phenomenon is not observed for wells with contraction because of the higher pressure drop after the contraction which dissipates the pressure wave.

Table 3. Dimensionless parameters used in geometric analysis.

| | One-cross-section well Kimura (2008) | Two-cross-section well | | | |
|---|---|---|---|---|---|
| | | Expansion | | Contraction | |
| | | Below | Above | Below | Above |
| $RA$ | $RA = 20000$ | $RA_1 = 10000$ | $RA_2 = 6666$ | $RA_1 = 6666$ | $RA_2 = 10000$ |
| Re | Re $= 400$ | Re$_1 = 400$ | Re$_2 = 600$ | Re$_1 = 600$ | Re$_2 = 400$ |
| $\beta$ | $\beta = 0.25$ | $\beta_1 = 0.25$ | $\beta_2 = 0.1818$ | $\beta_1 = 0.1818$ | $\beta_2 = 0.25$ |
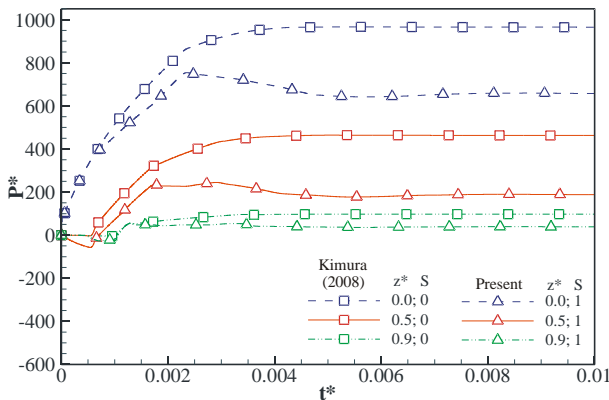


Figure 6. Time change of pressure for one-cross-section well ($S$=0) and two-cross-section well with expansion ($S$=1).
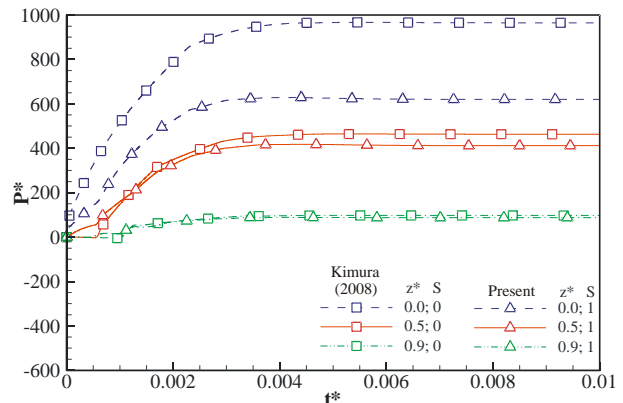


Figure 7. H Time change of pressure for one-cross-section well ($S$=0) and two-cross-section well with contraction ($S$=1).
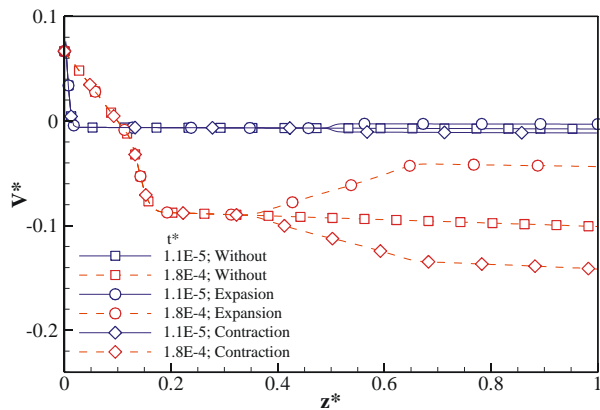


Figure 8. Average velocity field for two different instants.
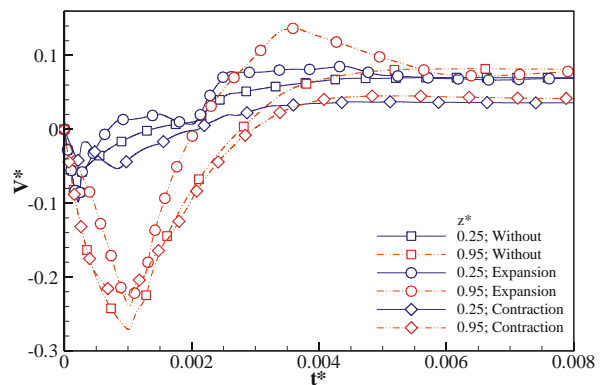


Figure 9. Time change of velocity for two different positions.

**4.3 Sensibility Analysis**

In all following simulations, there was a one expansion variation in the middle of the well. The effect of the well aspect ratio is now analyzed and the results are shown in Figure (10) and (11). The other dimensionless parameters were maintained at the following values: $\alpha^* = 1.27 \times 10^{-6}$, $Re_1 = 400$, $Re_2 = 600$, $\beta_1 = 0.25$ e $\beta_2 = 0.1818$. Figure 10 shows that the higher aspect ratio the higher the pressure values. Besides, oscillations of pressure are noted in shorter well which are pressure wave reflections. In high aspect ratio cases, the well is long enough to dissipate the pressure wave energy and the oscillations are diminished. This phenomenon is more evident in two-cross-section wells as pressure reflections also takes place at the cross-section changes.

Figure 11 shows that the effect of the aspect ratio on the average velocity fields. Note again that the pressure wave reflections are less evident in longer wells.
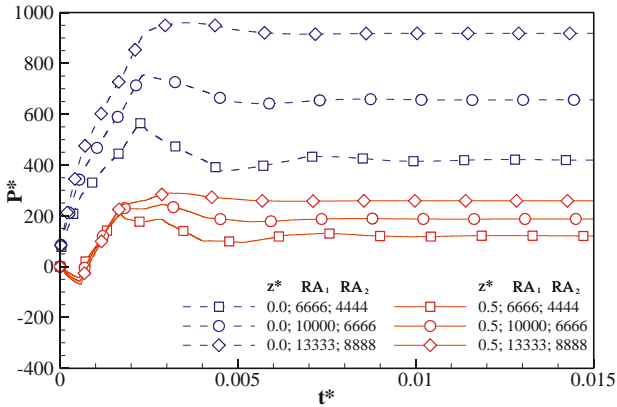
Figure 10. Time change of pressure at two positions for three different aspect ratios.
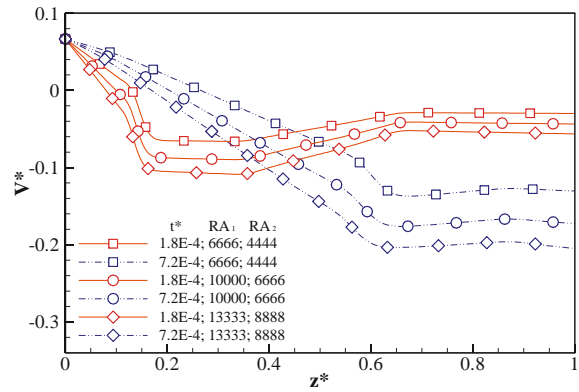


Figure 11. Velocity field for two different instants and three aspect ratios.

The effect of the Reynolds number was evaluated and the results are shown in Figures 12 and 13. According to Fig. 12, the higher the Reynolds number, the smaller the dimensionless pressure. One can see the effect of the cross sectional area is more pronounced for lower than for higher Reynolds numbers, as the change of slope at $z^*=0.5$ is more evident. Figure 13 shows that the maximum and the minimum values of the average velocity, are Reynolds number insensitive. However, the time for the system to reach the stead-state higher for higher Reynolds numbers. Higher Reynolds number need more time to dissipate the wave pressure energy.
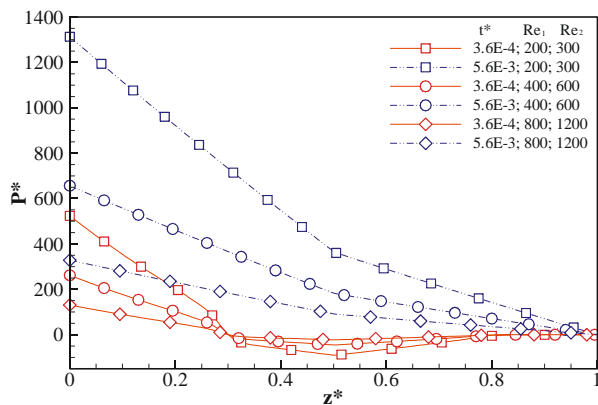


Figure 12. Pressure field for three Reynolds number at two different instants.
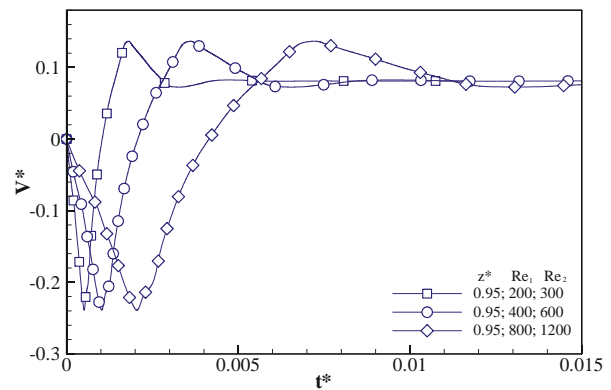


Figure 13. Time change of velocity for three Reynolds number at a position near the head.

The effect of the drill pipe-to-wellbore diameter ratio was evaluated by using the same diameter ratio below and above the cross-section change. As can be seen in Figure 14, the pressure increase with the diameter ratio (smaller $D_h$) because of the higher pressure drop caused by smaller annular spaces. However, the difference between the pressure peaks and the steady state value increase with the reduction of the diameter ratio. The reason for that is the larger change in the cross sectional area that cause higher pressure wave reflection.

At earlier times, the velocity field is only affected by the diameter ratio on the upper part of the well, as shown in Figure 15. Later, the whole velocity profile is affected by the diameter ratio change.

Figure 16 illustrates the pressure field for three different dimensionless compressibility values. Note that for smaller compressibility the pressure evolves faster along the well because of the smaller dissipation. The time for a pressure wave to reach the upper part of the well is smaller for smaller compressibility and the reflection in the cross-section change is more pronounced (see Figure 17). Because of this the average velocity does not reaches small values. However, the peak of velocity is higher for smaller compressibility.
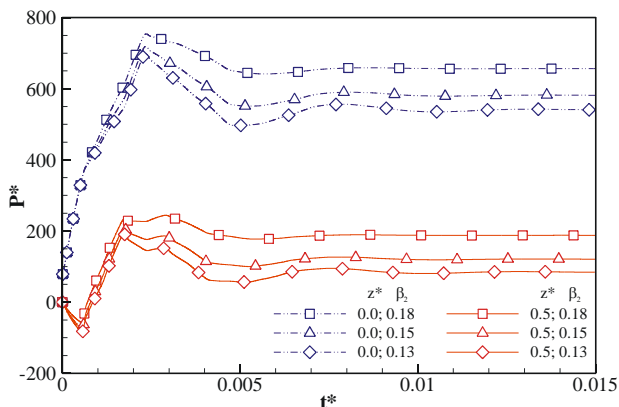
Figure 14. Time change of pressure for three diameter ratios at two different positions.
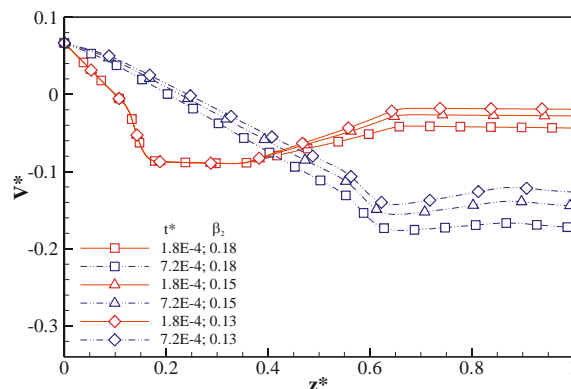


Figure 15. Velocity field for three diameter ratios at two different instants.
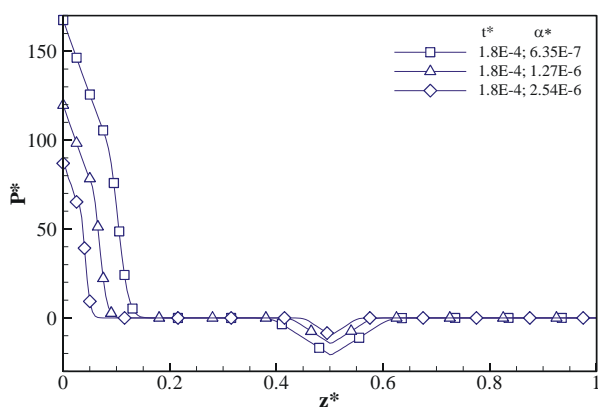


Figure 16. Pressure field for three dimensionless compressibility values.
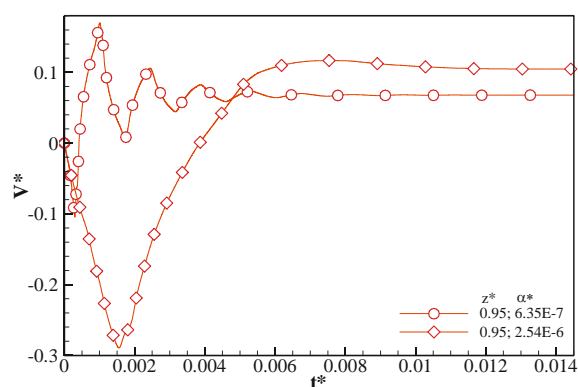


Figure 17. Time change of velocity for two dimensionless compressibility values.

## 5. CONCLUSION

In this paper, a mathematical model to predict surge and swab pressures in a vertical oil well with variation on cross-section is presented. The fluid is modeled as Newtonian with constant compressibility. The flow is assumed isothermal, one-dimensional and laminar. All simulations were performed with two-cross-section wells with the cross-section change at the middle of the well. The governing equations are solved by the Finite Volume Method.

The cross-section variation changes the pressure transmission, as part of pressure wave is reflected and the other transmitted at the cross-section change. This phenomenon causes higher peaks of pressure than those observed in a one-cross-section well. Besides, the time for the system to reach the steady state increases with the inclusion of the cross-section change.

In wells with an expansion, valleys of pressure are observed in positions downwind the expansion due to the local pressure drop. In wells with a contraction on the cross-section change, higher pressure gradients are noted in positions upwind the contraction due to the different pressure drop.

An interesting phenomenon observed is the dependence of the pressure with the ratio of cross sectional areas. This ratio does not change much the value of the peak pressure, but increase the time for the steady-state to be reached because of the pressure wave reflection at the cross-section change.

## 6. ACKNOWLEDGEMENTS

## 7. REFERENCES

Almeida, F. T. G. M. C. Sub e Sobrepressões Geradas Pelo Movimento Axial Transitório de Colunas de Perfuração. Mechanical Engineering Departament, UTFPR, Brazil, 2009.
Anderson, J. D. Modern Compressible Flow: With Historical Perspective. 2. ed. Estados Unidos: McGraw-Hill, 1990.
Assy, T. M. Mecânica dos fluidos: fundamentos e aplicações. 2ª edição. Rio de Janeiro. Editora LTC, 2004.

Bing, Z.; Kaiji, Z.; Qiji, Y. Equations Help Calculate Surge and Swab Pressures in Inclined Wells. Oil & Gas Journal, v. 93, n. 38, 1995.

Bing, Z.; Kaiji; Z. Dynamic Model Predicts Well Bore Surge and Swab Pressures. Oil & Gas Journal, v. 94, n. 53, 1996.

Bourgoyne, A. T.; Millheim, K. K.; Chenever, M. E. Applied Drilling Engineering, Estados Unidos: Sociedade de Engenheiros de Petróleo (SPE), 1991.

Burkhardt, J. A. Wellbore Pressure Surges Produced by Pipe Movement. SPE Drilling Engineering, v. 13, 1961.

Fontenot, J. E.; Clack, R. K. An Improved Method for Calculating Swab and Surge Pressures and Circulating Pressures in a Drilling Well. SPE Drilling Engineering, v. 14, n. 5, 1974.

Fortuna, A. O. Técnicas Computacionais para Dinâmica dos Fluidos: Conceitos Básicos e Aplicações. 1. ed. São Paulo: São Paulo University, 2000.

Kimura, H. F. Modelagem Transitória do Escoamento de Fluido Newtoniano Gerado Pela Movimentação Axial de Colunas de Perfuração de Poços de Petróleo. Mechanical Engineering Departament, UTFPR, Brazil, 2008.

Lal, M. Surge and Swab Modeling for Dynamic Pressures and Safe Trip Velocities. In: IADC/SPE Drilling Conference, 1983.

Maliska, C. R. Transferência de Calor e Mecânica dos Fluidos Computacional. 2ª ed. Rio de Janeiro: LTC, 2004.

Mitchell, R. F. Dynamic Surge/Swab Predictions. SPE Drilling Engineering, v. 6, n.4, p. 325-333, set. 1988.

Patankar, S. V. Numerical Heat Transfer and Fluid Flow. Hemisphere Publishing Corp, 1980.

Sampaio Jr., J. H. B. Aplicativo para Estimativa de Surge e Swab para Cenários UDW/formações frágeis. Report.

## 8. RESPONSIBILITY NOTICE

The authors are the only responsible for the printed material included in this paper.